CrystEngComm

COMMUNICATION

View Article Online
View Journal | View Issue

Cite this: *CrystEngComm*, 2017, **19**, 4147

Received 12th December 2016,
Accepted 23rd January 2017

DOI: 10.1039/c6ce02549h

rsc.li/crystengcomm

Nanostructured ZnO as a structural template for the growth of ZIF-8 with tunable hierarchical porosity for CO_2 conversion†

Min-Kyeong Kim,‡[a] Daeok Kim,‡[a] Jung Yoon Seo,[b] Onur Buyukcakir[a] and Ali Coskun*[ac]

We report a new approach to introduce hierarchical porosity into ZIF-8 by using three-dimensional nanostructured porous ZnO as a structural template. Importantly, the textural properties of these nanostructures can be tuned simply by varying the size of the polymeric templates used for the preparation of ZnO. Moreover, the growth of ZIF-8 crystals on ZnO and the resulting hierarchical porosity enabled enhanced catalytic activity for the conversion of CO_2 into cyclic carbonates through an atom economy reaction in high yields with exceptional product selectivity.

Metal–organic frameworks (MOFs) are crystalline porous materials containing metal ions or clusters coordinated to organic linkers.[1,2] Importantly, the topology, textural properties and functionality of MOFs can be tuned simply by varying their individual components.[3–6] Zeolitic imidazolate frameworks (ZIFs) have emerged as a new class of MOFs, which involves tetrahedral coordination of transition metal ions to the imidazole-based organic linkers in a zeolite-like topology.[7,8] Their high porosity, thermal/chemical stability, surface functionalities and versatile synthesis methodology enabled their utilization in various applications such as gas storage & separation,[9–11] catalysis,[12–14] sensor[15] and biomedical applications.[16–19]

While the microporosity of ZIFs is desirable for high guest selectivity and strong binding affinity, it could lead to poor mass transport kinetics, thus limiting their efficiency in heterogeneous catalysis, energy storage and gas storage & separation applications. Therefore, the preparation of MOFs possessing hierarchical pore structures with interconnected micro- and meso-pores could, in principle, address this problem.[20–22] In this interconnected network structure, micropores are expected to offer efficient binding sites for the guest molecules, whereas mesopores could enable fast mass transport kinetics. In this direction, the introduction of hierarchical porosity into ZIFs has become an important research topic in recent years. Various strategies such as post-synthetic etching of ZIF crystals,[23] templated-growth[24] and surfactant-based routes[25–27] have been employed to develop hierarchical porosity in ZIFs. In spite of these inspiring results, there still exists a need for a simple, general strategy to control pore size/shape and morphology of the hierarchical MOFs.

Recently, much attention has been given to the development of solvent-free synthetic strategies for the preparation of ZIFs *via* simple physical mixing of metal oxide and molten linker.[28–31] Owing to the fast synthesis time, solvent-free and atom economic nature, this approach has been extensively used to prepare various ZIF structures in the form of powder, films and nanostructures on various surfaces. For example, Ameloot *et al.*[28] have recently synthesized ZnO nanostructures coated with ZIF-8 using a solvent-free route.

Recently, Rassaei and coworkers have also demonstrated the formation of a thin ZIF-8 film on ZnO nanorods *via* solvent-assisted uniform distribution of organic linkers prior to the heat treatment without any solvent.[29] These results clearly demonstrate the possibility of using ZnO as a structural template for the growth of MOF crystals. Considering the vast number of synthetic strategies to tune the nanostructure of ZnO,[32] it could be a good direction to introduce hierarchical porosity and functionality into MOFs, which could also adopt the morphology of ZnO. More importantly, the resulting composite could inherit some of the unique properties of ZnO such as luminescence, electrical property, photoconductivity, thermal conductivity, photocatalytic activity,[32] thus creating highly functional materials. Moreover, the presence of ZIF-8 can also extend the applications of these materials to heterogeneous catalysis for the conversion of CO_2 into cyclic carbonates.[33–36]

[a] *Graduate school of EEWS, Korea Advanced Institute of Science and Technology (KAIST), 291 Daehak-ro, Yuseong-gu, Daejeon, 305-701, Republic of Korea. E-mail: coskun@kaist.ac.kr*
[b] *Global Nanotechnology Development Team, National NanoFab Center (NNFC), 291 Daehak-ro, Yuseong-gu, Daejeon 34141, Republic of Korea*
[c] *Department of Chemistry, KAIST, Daejeon 305-701, Republic of Korea*

† Electronic supplementary information (ESI) available: Materials and experimental methods. See DOI: 10.1039/c6ce02549h

‡ Both authors have equal contributions.

In this study, we have prepared (Fig. 1) ZIF-8/ZnO nanostructures with hierarchical porosity by growing ZIF-8 on the surface of meso/macroporous three-dimensional (3D) ZnO nanostructures. Our strategy for the synthesis and also for tuning the morphology of ZIF-8/ZnO nanostructure involves successive (1) self-assembly of polymer beads and ZnO nanoparticles, (2) pyrolysis to remove polymeric template and finally (3) the growth of ZIF-8 on the surface of ZnO nanostructure by reacting it with 2-methylimidazole (MIM) linker at 150 °C for 1 h. The resulting ZIF-8/ZnO nanostructures exhibited BET surface areas up to 243 $m^2 g^{-1}$ and high catalytic activity as a porous heterogeneous catalyst for the conversion of CO_2 into chloropropene carbonate in high yield with excellent product selectivity through an atom economy reaction. Importantly, the textural properties and functions of the resulting ZIF-8/ZnO nanostructures can be simply tailored by controlling the size and shape of templating polymer beads, which paves the way for the incorporation of tunable hierarchical porosity into ZIFs.

In order to demonstrate the effectiveness of this approach, we have synthesized ZnO nanostructures having different morphology and pore size by using different polymeric templates. Firstly, ZnO nanoparticles (27 nm) and spherical polymer beads (~220 nm, for ZnO(S) and ~5 μm, for ZnO(L)) were prepared by following well-established literature procedures.[37] Scanning electron microscopy (SEM) analysis of these particles revealed nearly mono-disperse particle size distribution (see Fig. S1, ESI†). The aqueous dispersions of as-prepared ZnO nanoparticles and polymer beads were mixed at a weight ratio of (1 : 5 for ZnO(S) and 1 : 15 for ZnO(L)) at room temperature and then vacuum filtrated on a nanoporous anionic alumina oxide film. Polymer/ZnO composites were obtained by drying the filtrates at 40 °C for 8 h. In order to remove the template and to form 3D crystalline ZnO nanostructures, polymer beads were removed by heating the composites at 450 °C under air for 4 h. Following the thermal treatment, SEM analysis of ZnO nanostructures revealed (Fig. 2a–d) the formation meso/macroporous structures.

Fig. 1 Schematic description of the preparation of hierarchical ZIF-8/ZnO nanostructures.

As prepared ZnO nanostructures were then used as structural templates and metal sources to form ZIF-8 on their surface. For the uniform and homogeneous formation of ZIF-8 on the ZnO surface,[29] we mixed 0.08 g of porous ZnO with 1 mL methanol solution of MIM (1 M) and then evaporated methanol slowly at room temperature. Subsequent heating step at 150 °C for 1 h was employed for the formation of ZIF-8. The resulting product was collected and washed with copious amount of methanol in order to remove any unreacted organic precursor. It is important to note that the solvent-assisted homogeneous dispersion of MIM on the ZnO nanostructure was found to be very critical for maintaining the porosity of ZnO nanostructure. When the same reaction on porous ZnO was carried out using MIM powder without any solvent, we observed blocking of the pores accompanied by the loss of meso/macropores of the ZnO nanostructure (see Fig. S2, ESI†). We have carried out SEM analysis to observe structural changes of ZnO nanostructures before and after ZIF-8 formation. SEM images of ZnO nanostructures synthesized using small and large polymeric templates showed particle size of a few tenth of μm (Fig. 2a–d), wherein ZnO nanoparticles were transformed into 3D porous networks. Importantly, we have observed different pore size and morphology for ZnO nanostructures depending on the size of polymeric templates. ZnO nanostructure constructed using 220 nm polymer bead, ZnO(S), showed average pore size of 144 nm with unimodal size distribution (see Fig. S3, ESI†). In addition, the usage of 5 μm polymer beads led to the formation of porous ZnO nanostructures with micron-sized channels, ZnO(L). Notably, the pores are interconnected throughout the structure and did not collapse after removing the polymer templates. SEM images of ZIF-8/ZnO nanostructures (Fig. 2e–h) revealed the retention of porous networks, thus showing that it is, in fact, possible to inherit nanostructure of the templating ZnO. It is noteworthy to mention that the generated porosity was retained even after through washing and evacuation process at 150 °C, an indication of enhanced stability of ZIF-8/ZnO nanostructures. In order to confirm the formation ZIF-8 on the surface of ZnO nanostructures, we have carried out powder X-ray diffraction (PXRD) analysis before and after the formation of ZIF-8. PXRD spectrum of ZnO revealed (Fig. 3a) highly crystalline diffraction peaks above $2\Theta = 30°$, corresponding to the (100), (002), (101) and (102) diffractions of ZnO.[8] After the formation of ZIF-8, ZIF-8/ZnO(S), new diffraction peaks were observed below $2\Theta = 30°$, matching well with the diffraction pattern of ZIF-8, along with ZnO peaks, thus proving the formation of ZIF-8 on the surface of ZnO nanostructure. These findings were further supported by the Fourier transform infrared spectroscopy (FT-IR), which showed the emergence of characteristic ZIF-8 peaks following its growth on the ZnO surface.

In order to further analyze the morphology of ZIF-8/ZnO(S) nanostructure, we have carried out transmission electron microscopy (TEM) measurement with electron dispersive

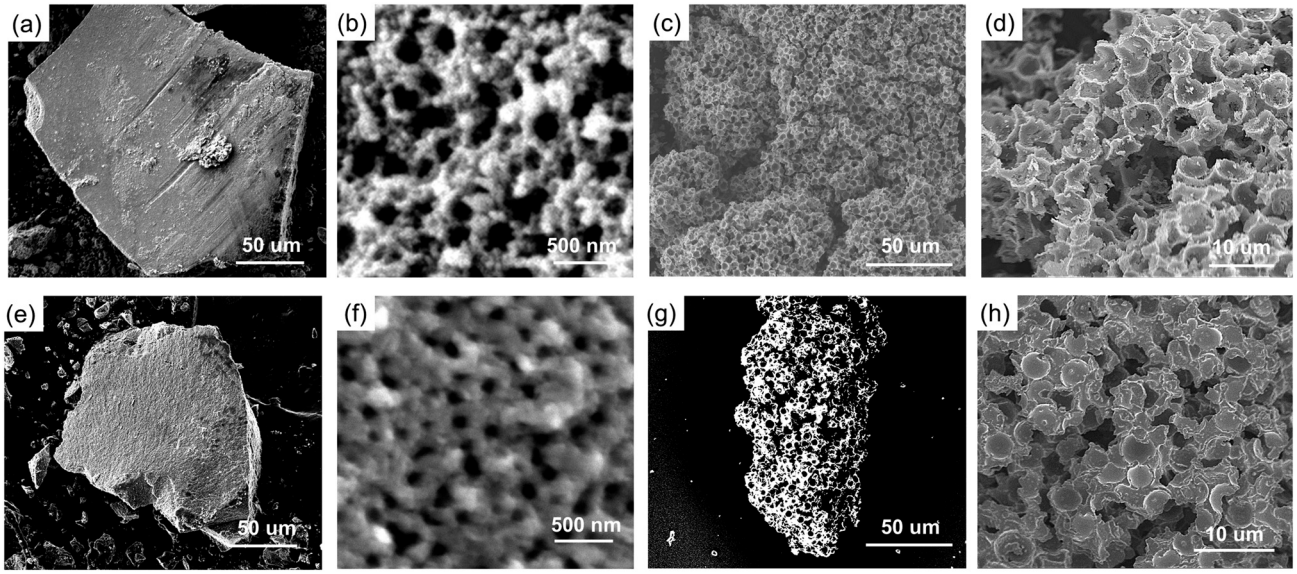

Fig. 2 SEM images of (a and b) ZnO(S) template, (c and d) ZnO(L) template, (e and f) ZIF-8/ZnO(S), and (g and h) ZIF-8/ZnO(L).

X-ray spectroscopy mapping (Fig. 4). We have observed voids larger than 50 nm surrounded by walls composed of spherical particles in the TEM image, confirming hierarchical porosity of the structure. Mapping of Zn, O and N elements on the TEM image, revealed their homogeneous distribution throughout the structure. While we had expected the appearance of ZnO/ZIF-8 core–shell structure due to the reaction of ZnO outer surface with MIM, the resulting structure seems to be the mixture of both ZIF-8 and ZnO on the surface.

The porosity of ZnO template and ZIF-8/ZnO nanostructures was investigated by measuring Ar adsorption–desorption isotherms (Fig. 5a) at 87 K. While ZnO templates did not show any noticeable porosity, ZnO/ZIF-8 nanostructures revealed the combination of type I and IV with a wide hysteresis loop at relative pressures above P/P_o = 0.3, indicating the presence of interconnected micro-mesoporous structure. ZIF-8/ZnO(S) and ZIF-8/ZnO(L) showed BET surface areas of 220 and 243 $m^2\ g^{-1}$, respectively, mainly originating from micropores (Fig. 5b) of *in situ* grown ZIF-8 crystals (micropore surface areas: 205 and 224 $m^2\ g^{-1}$, respectively). In order to investigate the origin of meso/macropores, we have carried out pore size distribution analysis using Barrett–Joyner–Halenda (BJH) method. In addition to the micropores (8–9 Å) originating from ZIF-8, the ZIF-8/ZnO(S) also showed mesopores ranging from 2.6 to 6 nm (Fig. 5b) due to the intercrystalline pores generated by the connection of ZIF-8 crystals. ZnO/ZIF-8(S) also showed larger pores ranging from 20–100 nm, whereas ZnO/ZIF-8(L) exhibited pores larger than 100 nm. Considering the big difference in the size of polymer beads (220 nm, for ZnO(S) *vs.* 5 μm, for ZnO(L)) used for building ZnO nanostructures, the appearance of large pores is assigned to the voids of ZnO nanostructures. These results collectively suggest the formation of ZIF-8/ZnO nanostructure with hierarchical porosity.

We further elaborated on the surface area of ZIF-8/ZnO composite with respect to the increasing the composition of ZIF-8. Accordingly, we increased the equivalent of MIM to 2 and 3 times and carried out the reactions with ZnO nanostructures. PXRD analysis of the resulting ZIF-8/ZnO nanocomposites showed similar diffraction peaks to those of ZIF-8/ZnO obtain at lower MIM concentrations regardless of the MIM ratio (see Fig. S4, ESI†). In addition, in the BET analysis (see Fig. S5, ESI†), we didn't observe any noticeable increase in the surface area. This result shows clearly that the ZIF

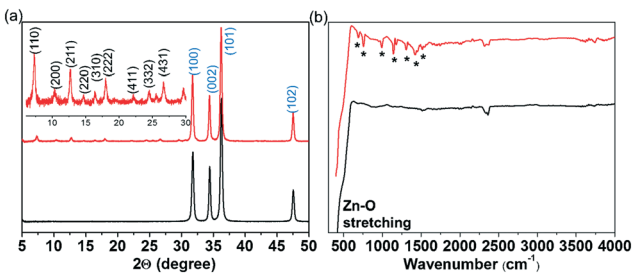

Fig. 3 (a) XRD and (b) FT-IR spectra of ZnO (black) and ZIF-8/ZnO (red) nanostructures.

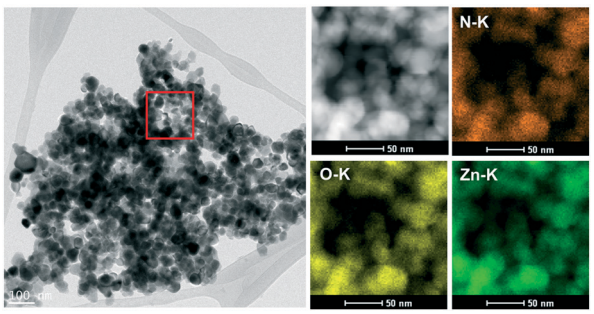

Fig. 4 Transmission electron microscopy (TEM) and energy dispersive spectroscopy (EDS) elemental mapping images of ZIF-8/ZnO(S) nanostructure.

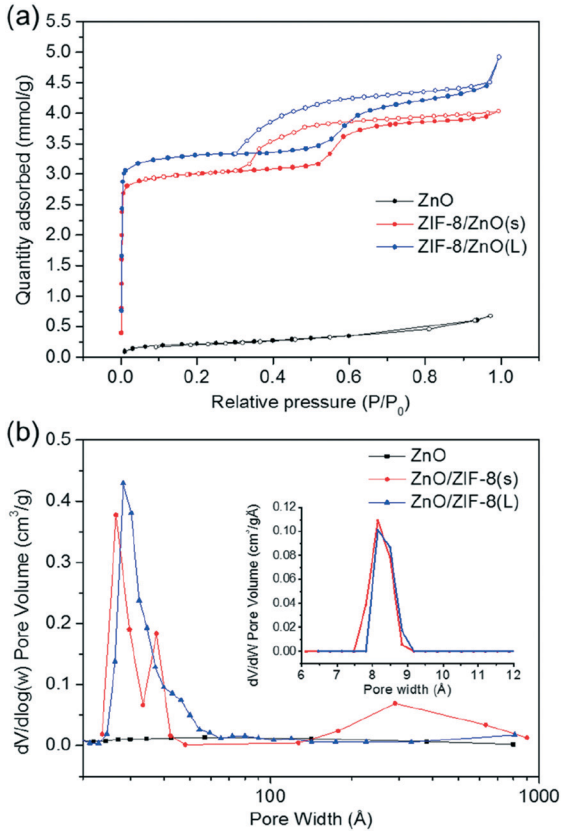

Fig. 5 (a) Ar adsorption–desorption isotherms of ZnO and ZIF-8/ZnO nanostructures at 87 K along with their (b) Barrett–Joyner–Halenda meso/macropore size distribution. Inset in (b) NLDFT micropore size distribution.

formation only occurs at the surface and once the surface is saturated additional MIM cannot be converted into ZIF-8.

Recently, ZIFs have emerged as promising porous heterogeneous catalysts for the conversion of CO_2 into cyclic carbonates through an atom economy reaction.[33–36] In particular, ZIF-8 has been shown to facilitate CO_2 conversion reaction under relatively mild reaction conditions without using any co-catalyst or solvents. It is, however, important to note that ZIF-8 mostly lost its catalytic activity even after one catalytic cycle and showed relatively low product selectivity leading to the formation of diols and dimers along with the desired cyclic carbonate.[35] We envisioned that the growth of ZIF-8 on the ZnO surface could not only improve its stability, but it could also improve its catalytic activity mainly due to enhanced mass transport kinetics through the meso/macropores of the ZIF-8/ZnO nanostructure. Accordingly, we explored the catalytic activity of ZIF-8/ZnO(S) (6 wt%) in the conversion of CO_2 using epichlorohydrin to form chloropropene carbonate under different reaction conditions and analyzed the resulting products by ^{1}H NMR analysis (see Table S1 and Fig. S6–S8, ESI†). Notably, we only observed the formation of chloropropene carbonate without the formation of any side products. We observed a strong dependence to both temperature and pressure in the conversion yields. For example, at 40 °C and 10 bar, we did not observe any product formation. Upon increasing the reaction temperature to 60 and 80 °C, we observed conversion yields of 30 and 70%, respectively. When the reaction temperature further increased to 100 °C, although we observed higher conversion yield of 83% in the 1st cycle, in the subsequent cycle, the formation of side products were also observed, which was accompanied by a decrease in the conversion yield. In an effort to optimize the reaction pressure, we also varied CO_2 pressure at 80 °C. We observed increasing conversion yields (13, 47 and 70% at 4, 7 and 10 bar, respectively) with rising pressure. Notably, these reactions conditions are in good agreement with those of the previously reported ZIF-8 based systems.[35] In order to analyze the role of ZnO on the catalytic activity, CO_2 conversion experiments were also conducted using ZnO. Importantly, ZnO showed (see Fig. S9, ESI†) no catalytic activity indicating that the catalytic activity of ZIF-8/ZnO nanostructure originates solely from the ZIF-8 crystals. To investigate the effect of pore size on the conversion yield of epichlorohydrin, we also conducted the CO_2 cycloaddition reaction using ZIF-8/ZnO(L) at 80 °C 10 bar. ZIF-8/ZnO(L) showed higher conversion yield of 87% (see Fig. S10, ESI†) compared to the ZIF-8/ZnO(S) (70%) under the same conditions, thus not only demonstrating the positive impact of hierarchical porosity, but also pointing to the possibility of tuning catalytic activity of MOFs by simply controlling the morphology of metal oxide template. We believe that the hierarchical porosity of ZIF-8/ZnO possessing interconnected micro-, meso- and micron-sized pores is contributing significantly to the efficient transport of reagents to the catalytic reaction sites and also facilitate the removal of products. In addition, the micrometer-sized particles also enable more convenient recovery of the catalyst after finishing the reaction and improves cyclability.

In order to investigate the catalytic stability of ZIF-8/ZnO(S), we carried out recyclability tests up to 4 cycles (see Fig. S11, ESI†). Unlike previously reported ZIF-8 based catalysts, ZIF-8/ZnO(S) showed complete retention of its catalytic activity in the 2nd cycle. In the subsequent cycles, we observed a decrease in conversion yields (3rd cycle, 39% and 4th cycle, 10%) while retaining high product selectivity. PXRD analysis of ZIF-8/ZnO(S) after the 4th cycle revealed (see Fig. S12, ESI†) a partial loss of crystallinity in ZIF-8, which could explain the origin of decreasing catalytic activity. It is, however, important to note that we still observed significant enhancement in catalytic activity compared to ZIF-8 in terms of both conversion yields and product selectivity,[35] thus demonstrating the viability of using metal oxides as structural templates for the MOF growth.

In summary, we have demonstrated the efficient growth of MOF crystals on the surface of nanostructured metal oxides. Importantly, the MOF structure has been shown to inherit surface morphology of the metal oxide structural template, thus providing a powerful tool to introduce hierarchical porosity into various MOF structures. In addition, the combination of MOFs and ZnO is expected to impart new emergent properties to the resulting nanostructures such as enhanced

stability and catalytic activity for catalytic, environmental and energy storage applications.

Acknowledgements

This work was supported by a National Research Foundation of Korea (NRF) grant funded by the Korean government (MEST) (NRF-2014R1A4A1003712 and BK21 PLUS program.

Notes and references

1 J. L. C. Rowsell and O. M. Yaghi, *Microporous Mesoporous Mater.*, 2004, **73**, 3–14.
2 H. C. Zhou, J. R. Long and O. M. Yaghi, *Chem. Rev.*, 2012, **112**, 673–674.
3 D. N. Bunck and W. R. Dichtel, *Chem. – Eur. J.*, 2013, **19**, 818–827.
4 T. H. Chen, I. Popov, W. Kaveevivitchai and O. S. Miljanic, *Chem. Mater.*, 2014, **26**, 4322–4325.
5 G. Kaur, R. K. Rai, D. Tyagi, X. Yao, P. Z. Li, X. C. Yang, Y. L. Zhao, Q. Xu and S. K. Singh, *J. Mater. Chem. A*, 2016, **4**, 14932–14938.
6 M. Kim, J. F. Cahill, H. H. Fei, K. A. Prather and S. M. Cohen, *J. Am. Chem. Soc.*, 2012, **134**, 18082–18088.
7 B. L. Chen, Z. X. Yang, Y. Q. Zhu and Y. D. Xia, *J. Mater. Chem. A*, 2014, **2**, 16811–16831.
8 K. S. Park, Z. Ni, A. P. Cote, J. Y. Choi, R. D. Huang, F. J. Uribe-Romo, H. K. Chae, M. O'Keeffe and O. M. Yaghi, *Proc. Natl. Acad. Sci. U. S. A.*, 2006, **103**, 10186–10191.
9 Y. C. Pan, T. Li, G. Lestari and Z. P. Lai, *J. Membr. Sci.*, 2012, **390**, 93–98.
10 S. R. Venna and M. A. Carreon, *J. Am. Chem. Soc.*, 2010, **132**, 76–78.
11 H. Wu, W. Zhou and T. Yildirim, *J. Am. Chem. Soc.*, 2007, **129**, 5314–5315.
12 U. P. N. Tran, K. K. A. Le and N. T. S. Phan, *ACS Catal.*, 2011, **1**, 120–127.
13 L. H. Wee, T. Lescouet, J. Ethiraj, F. Bonino, R. Vidruk, E. Garrier, D. Packet, S. Bordiga, D. Farrusseng, M. Herskowitz and J. A. Martens, *ChemCatChem*, 2013, **5**, 3562–3566.
14 F. Zhang, Y. Y. Wei, X. T. Wu, H. Y. Jiang, W. Wang and H. X. Li, *J. Am. Chem. Soc.*, 2014, **136**, 13963–13966.
15 G. Lu, O. K. Farha, W. N. Zhang, F. W. Huo and J. T. Hupp, *Adv. Mater.*, 2012, **24**, 3970–3974.
16 P. Horcajada, R. Gref, T. Baati, P. K. Allan, G. Maurin, P. Couvreur, G. Ferey, R. E. Morris and C. Serre, *Chem. Rev.*, 2012, **112**, 1232–1268.
17 K. Liang, C. J. Coghlan, S. G. Bell, C. Doonan and P. Falcaro, *Chem. Commun.*, 2016, **52**, 473–476.
18 K. Liang, R. Ricco, C. M. Doherty, M. J. Styles, S. Bell, N. Kirby, S. Mudie, D. Haylock, A. J. Hill, C. J. Doonan and P. Falcaro, *Nat. Commun.*, 2015, **6**, 7240.
19 K. Liang, J. J. Richardson, J. W. Cui, F. Caruso, C. J. Doonan and P. Falcaro, *Adv. Mater.*, 2016, **28**, 7910–7914.
20 P. Li, J. A. Modica, A. J. Howarth, E. Vargas, P. Z. Moghadam, R. Q. Snurr, M. Mrksich, J. T. Hupp and O. K. Farha, *Chem*, 2016, **1**, 154–169.
21 Y. Li, Z. Y. Fu and B. L. Su, *Adv. Funct. Mater.*, 2012, **22**, 4634–4667.
22 C. M. A. Parlett, K. Wilson and A. F. Lee, *Chem. Soc. Rev.*, 2013, **42**, 3876–3893.
23 C. Avci, J. Arinez-Soriano, A. Carne-Sanchez, V. Guillerm, C. Carbonell, I. Imaz and D. Maspoch, *Angew. Chem., Int. Ed.*, 2015, **54**, 14417–14421.
24 H. L. Huang, J. R. Li, K. K. Wang, T. T. Han, M. M. Tong, L. S. Li, Y. B. Xie, Q. Y. Yang, D. H. Liu and C. L. Zhong, *Nat. Commun.*, 2015, **6**, 8847.
25 J. Cravillon, R. Nayuk, S. Springer, A. Feldhoff, K. Huber and M. Wiebcke, *Chem. Mater.*, 2011, **23**, 2130–2141.
26 S. C. Junggeburth, K. Schwinghammer, K. S. Virdi, C. Scheu and B. V. Lotsch, *Chem. – Eur. J.*, 2012, **18**, 2143–2152.
27 Y. N. Wu, M. M. Zhou, B. R. Zhang, B. Z. Wu, J. Li, J. L. Qiao, X. H. Guan and F. T. Li, *Nanoscale*, 2014, **6**, 1105–1112.
28 I. Stassen, N. Campagnol, J. Fransaer, P. Vereecken, D. De Vos and R. Ameloot, *CrystEngComm*, 2013, **15**, 9308–9311.
29 H. Al-Kutubi, A. Dikhtiarenko, H. R. Zafarani, E. J. R. Sudholter, J. Gascon and L. Rassaei, *CrystEngComm*, 2015, **17**, 5360–5364.
30 M. Lanchas, S. Arcediano, A. T. Aguayo, G. Beobide, O. Castillo, J. Cepeda, D. Vallejo-Sanchez and A. Luque, *RSC Adv.*, 2014, **4**, 60409–60412.
31 J. B. Lin, R. B. Lin, X. N. Cheng, J. P. Zhang and X. M. Chen, *Chem. Commun.*, 2011, **47**, 9185–9187.
32 Z. L. Wang, *J. Phys.: Condens. Matter*, 2004, **16**, R829–R858.
33 J. Kim, S. N. Kim, H. G. Jang, G. Seo and W. S. Ahn, *Appl. Catal., A*, 2013, **453**, 175–180.
34 R. R. Kuruppathparambil, R. Babu, H. M. Jeong, G.-Y. Hwang, G. S. Jeong, M.-I. Kim, D.-W. Kim and D.-W. Park, *Green Chem.*, 2016, **18**, 6349–6356.
35 C. M. Miralda, E. E. Macias, M. Q. Zhu, P. Ratnasamy and M. A. Carreon, *ACS Catal.*, 2012, **2**, 180–183.
36 M. Q. Zhu, D. Srinivas, S. Bhogeswararao, P. Ratnasamy and M. A. Carreon, *Catal. Commun.*, 2013, **32**, 36–40.
37 H. W. Huang, J. Liu, G. F. He, Y. Peng, M. Wu, W. H. Zheng, L. H. Chen, Y. Li and B. L. Su, *RSC Adv.*, 2015, **5**, 101910–101916.